Inorganic Chemistry

ARTICLE

pubs.acs.org/IC

An Interpenetrated Metal−Organic Framework and Its Gas Storage Behavior: Simulation and Experiment

Daniela Frahm, Michael Fischer, Frank Hoffmann, and Michael Fröba*

Institute of Inorganic and Applied Chemistry, Department of Chemistry, University of Hamburg, Martin-Luther-King-Platz 6, D-20146 Hamburg, Germany

Supporting Information

ABSTRACT: A new metal−organic framework, called UHM-6 (UHM: University of Hamburg Materials), based on the copper paddle wheel motif and a novel organosilicon linker, 4′,4″-(dimethylsilanediyl)bis-(biphenyl-3,5-dicarboxylic acid) (**sbbip**), has been synthesized and characterized with regard to its gas storage behavior up to 1 bar for hydrogen, methane, and carbon dioxide. The 2-fold interpenetrated microporous framework of UHM-6 is isoreticular to PMOF-3 (*Inorg. Chem.* **2009**, *48*, 11507) and is composed of cuboctahedral cages of Cu_2 paddle wheels connected via nonlinear organosilicon units. The structure (*SG I*422, No. 97) is characterized by straight channels running along the [001] and [110] direction. UHM-6 reveals a specific surface area of $S_{BET} \sim 1200\ m^2\ g^{-1}$ and a specific micropore volume of $V_{micropore} \sim 0.48\ cm^3\ g^{-1}$. At 1 bar the activated form of UHM-6 shows a hydrogen uptake of 1.8 wt % (77 K), a methane uptake of 0.8 mmol g^{-1} (293 K), and a carbon dioxide uptake of 3.3 mmol g^{-1} (273 K). Accompanying theoretical grand-canonical Monte Carlo (GCMC) simulations show an overall good agreement with the experimental results. Furthermore, GCMC adsorption simulations for three binary equimolar mixtures (CH_4/H_2, CO_2/H_2, and CO_2/CH_4) were carried out (T = 298 K) to assess the potential for gas separation/purification applications.

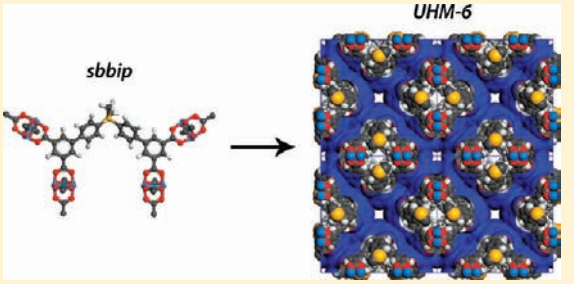

INTRODUCTION

In the light of global warming, there is a strong need for using alternative clean-burning fuels to reduce the carbon dioxide emissions. Among various alternatives, particularly hydrogen has emerged as a potential candidate to replace fossil fuels. Apart from the fact that this replacement is only meaningful if hydrogen would be produced using renewable energies there are several other problems to solve; concerning the private transport sector, the most prominent would be to develop an efficient and safe storage system which is still missing.[1,2] The use of hydrogen physisorption on porous materials is one of the main methods being considered as a possible solution. Besides research on long-known porous materials such as zeolites or carbons there is a more recent and rapidly growing research interest on the synthesis and characterization of a new class of inorganic−organic hybrid materials called metal−organic frameworks (MOFs) or porous coordination polymers (PCPs).[3−5] Exhibiting properties like exceptionally high specific surface areas, large inner pore volumes, and tunable pore sizes, it is their modular design, being composed of multidentate variable organic ligands as linkers coordinating to metal ions or metal clusters (so-called connectors), what makes MOFs unique.[6] MOFs are considered as potential candidates for usage in a wide range of applications, not only in physisorption based gas storage but also in gas separation and catalysis.[7−10]

Concerning gas storage capacity, there are a lot of different characteristics that influence the physisorption behavior in MOFs. Particularly the behavior of hydrogen as an adsorptive has been already intensively studied to tailor a MOF that is capable of meeting the U.S. Department of Energy (DoE) performance targets for hydrogen storage systems.[11] In computer based simulation studies Frost et al. were able to identify three adsorption regimes for a series of MOFs with the same topology but different pore sizes: at low pressure (loading), the hydrogen uptake correlates with the heat of adsorption, at intermediate pressure, uptake correlates with the specific surface area while at high pressures, the uptake correlates with the free inner volume.[12] The adsorption behavior can be further influenced by the incorporation of unsaturated metal sites (like in the well-known copper paddlewheel motif) which show a rather strong and local interaction toward hydrogen.

The optimization of the pore sizes and overall topology of MOFs to maximize the hydrogen uptake is closely associated with the choice of the linker.[13−15] In this respect, the group of nonlinear/bent and conformationally flexible linkers is interesting as they enable the formation of uncommon or even hitherto unknown topologies. In PCN-12, currently being the world record holder in low pressure hydrogen storage (3.05 wt % at 1 bar), the linker 5,5′-methylene-di-isophtalate (mdip) is incorporated in two different conformations: one in which the two phenyl rings face each other (symmetry C_{2v}) and another one, in

Received: July 25, 2011
Published: October 10, 2011

which the phenyl rings are oriented perpendicular to each other (symmetry C_s).[16] This enables the formation of cuboctahedral cages in which the open metal sites are aligned in a way that they can interact directly with the species inside the void and thus enhance the isosteric heat of adsorption. This motif is also realized in a series of MOFs, UHM-2, UHM-3 (aka PCN-12-Si), and UHM-4 (UHM: University of Hamburg Materials), which are all isoreticular to PCN-12 and in which the central methylene unit is substituted by a isopropylidene, dimethylsilanediyl, and dimethylgermandiyl unit, respectively.[17,18] Furthermore, Pan and co-workers also employed a nonlinear linker with a sp^3-hybridized carbon center. The linker 4,4′-(hexafluoroisopropylidene)bis(benzoic acid) (H_2hfipbb) is characterized by six fluorine atoms at the sp^3-center and gives rise to a 2-fold interpenetrated three-dimensional MOF structure [Cu(hfipbb)-(H_2Hfipbb)$_{0.5}$]with perfectly ordered one-dimensional (1D) channels. Interestingly, the linker is incorporated into this structure in only one conformation (C_1 symmetry). It has already been shown that interpenetration can be a method for enhancing the gas storage capacity of MOFs as well.[19] In addition Cu(hfipbb)-(H_2Hfipbb)$_{0.5}$ exhibit very interesting properties concerning the separation of various volatile organic compounds (VOCs).[20,21]

Here, we present the synthesis and characterization of a new organosilicon linker, exhibiting two isophtalic acid units bridged over two phenyl rings and a central dimethylsilanediyl unit, as well as the resulting copper based MOF, called UHM-6. The linker of UHM-6 is an extended version of the recently published linker 5,5′-(dimethylsilanediyl)diisophthalic acid (dmsdip) which was employed in the synthesis of UHM-3 (PCN-12-Si).[17] This work is part of an ongoing project in which it is intended to investigate systematically the influence of the structure, conformation, and length of nonlinear linkers on the resulting network topology, the pore structure as well as gas storage and gas separation properties. The new MOF has been thoroughly characterized via powder X-ray diffraction (PXRD) measurements in combination with computational modeling techniques, thermal analysis (TG/DTA), N_2 physisorption measurements and further gas sorption studies (H_2, CH_4, CO_2) as well as corresponding force-field based Grand-canonical Monte Carlo (GCMC) simulations.

EXPERIMENTAL SECTION

Chemicals. 1,4-dibromobenzene (Sigma-Aldrich, 98%), *n*-butyl lithium (Sigma-Aldrich, 1.6 M in *n*-hexane), dichlorodimethylsilane (Merck, ≥ 98.0%), 3,5-dimethylphenylboronic acid (ABCR, 97%), tetrakis(triphenylphosphine)palladium(0) (ABCR, 99.9%) and potassium permanganate (Fluka, ≥ 99.0%) were used without further purification. Pyridine (Applichem, 99.0%) and *N*,*N*-dimethylformamide (DMF) (Grüssing, 99.5%) were used after purification by distillation; *N*, *N*-dimethylacetamide (DMA) (Sigma-Aldrich, ≥ 99.5%) was used as obtained.

Methods. NMR spectra were acquired using a Bruker AVANCE 400 or a Varian Gemini-200BB spectrometer. Infrared spectra were recorded with a Bruker Vertex 70 FT-IR spectrometer. PXRD patterns were obtained at room temperature using a STOE STADI P transmission powder diffractometer with Cu K_α radiation (40 kV, 30 mA, counting time 20 s, steps: 0.1° (2θ)). Thermal analysis (TG (thermogravimetry)/MS (mass spectrometry)) was carried out under O_2/Ar (20/80) flow (20 mL min^{-1}) with a NETZSCH STA 449 F3 Jupiter coupled by capillary with a Aëolos QMS 403 mass spectrometer. The heating rate was 5 K min^{-1} from room temperature to 700 °C.

The nitrogen physisorption measurements were conducted with a Quantachrome Quadrasorb SI-MP at 77 K. The argon physisorption measurements were conducted with a Quantachrome Autosorb 1-MP at 87 K. Using the Brunauer−Emmett−Teller (BET) method, the specific surface area was calculated from the adsorption branch in the relative pressure interval from 0.01 to 0.05. The micropore volume was estimated from the quantity of gas adsorbed at a relative pressure of 0.2. Volumetric hydrogen physisorption data were recorded on a Quantachrome Autosorb 1-C (purity of helium and hydrogen: 99.999%). Carbon dioxide and methane physisorption data were recorded on a Quantachrome Autosorb iQ (purity of carbon dioxide: 99.5%, purity of methane: 99.9995%).

Synthesis of the Linker. *Bis(4-bromphenyl)dimethylsilane (**1**).* The synthesis of (**1**) was carried out according to a literature procedure[22] under nitrogen atmosphere using dried solvents. At 0 °C 50.5 mL (80.8 mmol) of a *n*-butyl lithium solution (1.6 M in *n*-hexane) was added dropwise to 19.1 g (81.0 mmol) of 1,4-dibromobenzene dissolved in 300 mL of diethyl ether. After stirring at 0 °C for 2 h 4.90 mL (40.6 mmol) of dichlorodimethylsilane in 10 mL of diethyl ether were added dropwise. Afterward, the mixture was heated to room temperature and stirred for 16 h. The reaction mixture was separated from the resulting precipitate by filtration, washed twice with water, and dried over anhydrous sodium sulfate. Finally the solvent was evaporated in vacuum and recrystallized from ethyl acetate to give 14.3 g (38.6 mmol, yield: 96%) of a colorless crystalline powder.

^{1}H NMR ($CDCl_3$, 400 MHz): δ [ppm]: 7.48 (d, 4H), 7.33 (d, 4H), 0.52 (s, 6H); ^{13}C NMR ($CDCl_3$, 400 MHz): δ [ppm]: 136.4, 135.6, 131.0, 124.2, −2.6; IR [cm^{-1}]: 3068, 3031, 3012, 2961, 1647, 1567, 1477, 1376, 798, 723.

*Bis(3′,5′-dimethylbiphenyl-4-yl)dimethylsilane (**2**).* Under nitrogen atmosphere 10.0 g (27.1 mmol) of (**1**) were dissolved in 150 mL of *N*,*N*-dimethylformamide (DMF). After addition of 10.2 g (68.0 mmol) of 3,5-dimethylphenylboronic acid, 3.21 g (2.78 mmol) of tetrakis-(triphenylphosphine)-palladium(0) and 126 mL of sodium carbonate solution (20 wt % in water) the reaction mixture was stirred at 110 °C for 24 h. Afterward, the reaction mixture was treated with saturated aq. sodium chloride solution, filtrated, and extracted with *n*-hexane. After drying the organic phase over sodium sulfate, the solvent was evaporated in vacuum. The raw product was purified by column chromatography with *n*-hexane to give 5.27 g (12.5 mmol, yield: 46%) of a colorless highly viscous oil.

^{1}H NMR ($CDCl_3$, 400 MHz): δ [ppm]: 7.71 (q, 8H), 7.33 (d, 4H), 7.10 (s, 2H), 2.48 (s, 12H), 0.72 (s, 6H); ^{13}C NMR ($CDCl_3$, 400 MHz): δ [ppm]: 142.4, 141.3, 138.4, 136.9, 134.8, 129.3, 126.8, 125.3, 21.4, −2.3; IR [cm^{-1}]: 3064, 3017, 2955, 2862, 1599, 1468, 1382, 832, 820.

*4′,4″-(Dimethylsilanediyl)bis(biphenyl-3,5-dicarboxylic acid) (**3**).* The synthesis of (**3**) was carried out on the basis of a literature procedure.[23] 2.05 g (13.0 mmol) of potassium permanganate dissolved in 100 mL of water were added to a solution of 5.27 g (12.5 mmol) of (**2**) in 100 mL of pyridine, and the mixture was heated to 95 °C. Further 38.0 g of potassium permanganate were added slowly over 5 h. After stirring at 95 °C for 22 h the resulting manganese(IV) oxide was removed by filtration and washed with saturated sodium bicarbonate. The combined pyridine and sodium bicarbonate phase was extracted with ethyl acetate. The separated aqueous phase was acidified with diluted hydrochloric acid to precipitate the product. After filtration, recrystallization from ethanol/water (9:1) and drying in vacuum 4.38 g (8.12 mmol, yield: 65%) of a colorless crude powder was obtained.

^{1}H NMR (DMSO-d6, 400 MHz): δ [ppm]: 8.46 (s, 2H), 8.37 (d, 4H), 7.72 (dd, 8H), 0.61 (s, 6H); ^{13}C NMR (DMSO-d6, 400 MHz): δ [ppm]: 166.6, 140.8, 139.2, 137.7, 134.8, 132.4, 131.2, 129.1, 126.4, −2.3; IR [cm^{-1}]: 3410, 3070, 3020, 2955, 1696, 1600, 810, 774, 759.

Synthesis of UHM-6. In a typical synthesis 600 mg (1.11 mmol) of 4′,4″-(dimethylsilanediyl)bis(biphenyl-3,5-dicarboxylic acid) was dissolved

in 15 mL of DMA in a 50 mL flask and heated to 100 °C. Afterward, 0.536 g (2.22 mmol) of copper(II) nitrate trihydrate dissolved in 10 mL of DMA containing 5 drops of hydrochloric acid (37%) were added dropwise, and the mixture was stirred at 100 °C for 24 h. The resulting blue precipitate was collected by filtration, washed twice with DMA, and dried in vacuum (yield 720 mg). For activation the *as synthesized* form of the MOF was suspended for 48 h in methanol and then for 48 h in dichloromethane. In both cases the solvents were replaced by fresh solvents after 24 h. After the solvent exchange the MOF was thermally activated in vacuum for 24 h at 120 °C.

Computational Details. The accessible surface area of UHM-6 was calculated using the "Atom Volumes and Surfaces" tool of Accelrys Materials Studio, using a probe molecule radius of 1.84 Å.[24,25] The pore volume was obtained from a GCMC simulation of helium adsorption in UHM-6, using the procedure and the parameters described in a previous publication.[26] Grand-canonical Monte Carlo (GCMC) simulations of single-component and binary mixture adsorption in UHM-6 were carried out using the Sorption module of Accelrys Materials Studio package.[25] In analogy to experimental measurements, single-component isotherms were computed for $T = 77$ K for hydrogen, and for $T = 298$ K for methane and carbon dioxide. Mixture isotherms were calculated for the three binary mixtures of these gases, assuming an equimolar mixture composition, $T = 298$ K. In all calculations, pressures up to 1 bar were considered.

At least 2×10^6 equilibration steps and 2×10^6 production steps were used in the simulations of single-component adsorption, whereas 10×10^6 equilibration steps and 25×10^6 production steps were used for the binary mixtures. Both van der Waals (vdW) interactions and electrostatic interactions were included for all adsorbates. A cutoff radius of 12.5 Å was employed for vdW interactions, which were modeled using the Lennard-Jones (LJ) potential, together with Lorentz−Berthelot mixing rules to calculate the parameters for interactions between different atom types. Ewald summation was used to account for the periodicity of the lattice in the computation of electrostatic contributions.

All LJ parameters to model the framework atoms were taken from the Universal Force Field (UFF).[27] Framework charges were obtained from density functional theory (DFT) calculations for molecular model systems using the ESP method,[28] which are described in more detail in the Supporting Information. The LJ parameters for the hydrogen molecule were taken from the work of Buch, which employs a united-atom description.[29] LJ parameters from the TraPPE force field were employed for methane,[30] and the parameters proposed by García-Sánchez et al. were used for carbon dioxide.[31] To account for electrostatic interactions, a model consisting of three point charges was used to account for the quadrupole moment of H_2, which has been employed in a previous work.[26] For CH_4 and CO_2, ESP charges were obtained from DFT calculations. All LJ parameters and partial charges are given in the Supporting Information.

While the simulations deliver the absolute amount adsorbed, only the excess amount is accessible through experiment. Therefore, the absolute values n_{abs} obtained from the simulations were converted into excess quantities n_{exc} using the equation:

$$n_{exc}(p) = n_{abs}(p) - V_p \cdot \rho(p)$$

Here, V_p corresponds to the free pore volume obtained from the simulations of He adsorption, and $\rho(p)$ is the bulk gas density at the given pressure.

RESULTS AND DISCUSSION

Synthesis of the MOF UHM-6. The synthesis of the MOF UHM-6 is carried out in a flask by heating the linker sbbip (Scheme 1) and copper(II) nitrate trihydrate with DMA as a solvent, and results in a blue powder. To remove the solvent molecules remaining in the framework the *as synthesized* form of the MOF is activated by solvent exchange with methanol and dichloromethane followed by a thermal activation (120 °C, 24 h) in vacuum. The activation procedure leads to the microporous MOF UHM-6.

Scheme 1. Structural Formula of the New Organosilicon Linker 4′,4″-(dimethylsilanediyl)bis(biphenyl-3,5-dicarboxylic acid) (sbbip)[a]

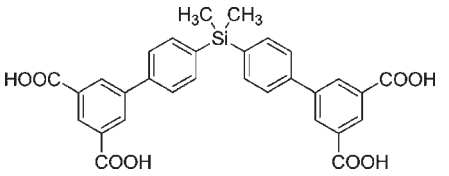

[a] The complete synthesis scheme is given in the Supporting Information.

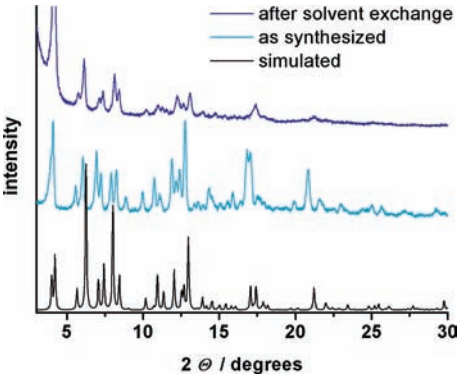

Figure 1. Comparison of the powder X-ray diffractograms of the simulated (black), the *as synthesized* (turquoise), and the solvent-exchanged (blue) sample of UHM-6.

PXRD and Structure Modeling. The crystal size of the synthesized UHM-6 compound was too small to allow single-crystal X-ray diffraction studies. However, the structure could be solved by using molecular modeling techniques in conjunction with the comparison to experimental PXRD data. The structure of UHM-6 was modeled in analogy to the procedure described by Loiseau et al.,[32] that is, by applying a sort of "homology modeling", using the structure of PMOF-3[33] as a starting point. However, no a priori space group restrictions were applied. First, the original linker was substituted with the new linker sbbip (Scheme 1). After removing any symmetry restrictions the constructed model was submitted to a full energy minimization, including optimization of the unit cell dimension and metric, with parameters from the UFF as implemented in the Materials Studio package. The vdW interactions (represented by a classical 12−6 Lennard-Jones potential) beyond 12.5 Å were neglected. The convergence criteria were set to 2.0×10^{-5} kcal mol^{-1} and 0.001 kcal mol^{-1} Å^{-1}, respectively. The geometry optimization converged to result in a plausible tetragonal structure with the space group $I422$, No. 97 ($a = b = 31.1560$ Å, $c = 28.2315$ Å, $\alpha = \beta = \gamma = 90°$, $V = 27{,}404$ Å^3). In Figure 1 the experimental and simulated PXRD patterns are compared. The differences between the simulated and the experimental *as synthesized* XRD pattern are related mainly to the (relative) intensities and resolution of the reflections, while the positions are in excellent agreement

dx.doi.org/10.1021/ic201596x |*Inorg. Chem.* 2011, 50, 11055–11063

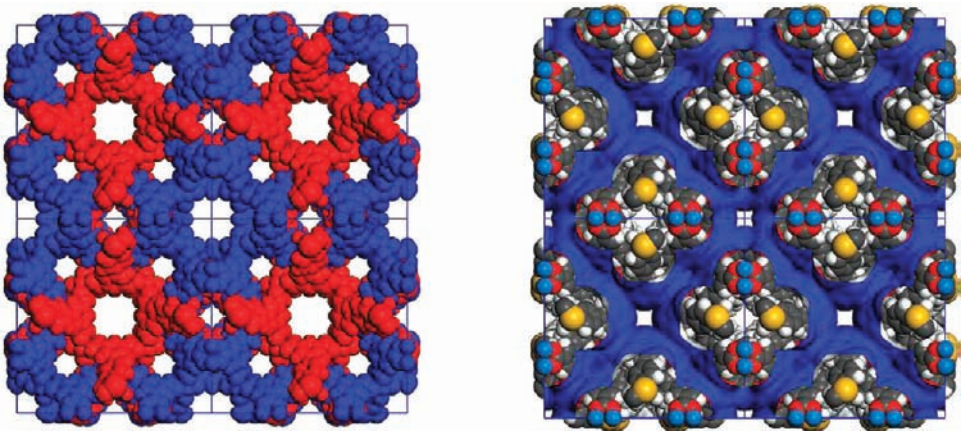

Figure 2. (left) Four unit cells with a view along the *c*-axis of UHM-6 and the visualization of the 2-fold interpenetrated structure. The two frameworks (red and blue) are related to each other by a translation of ($^1/_2$, $^1/_2$, $^1/_2$). (right) Accessible surface area (denoted in blue) of UHM-6 and the straight channels running along the [001] direction; gray: carbon, white: hydrogen, red: oxygen, blue: copper, and yellow: silicon.

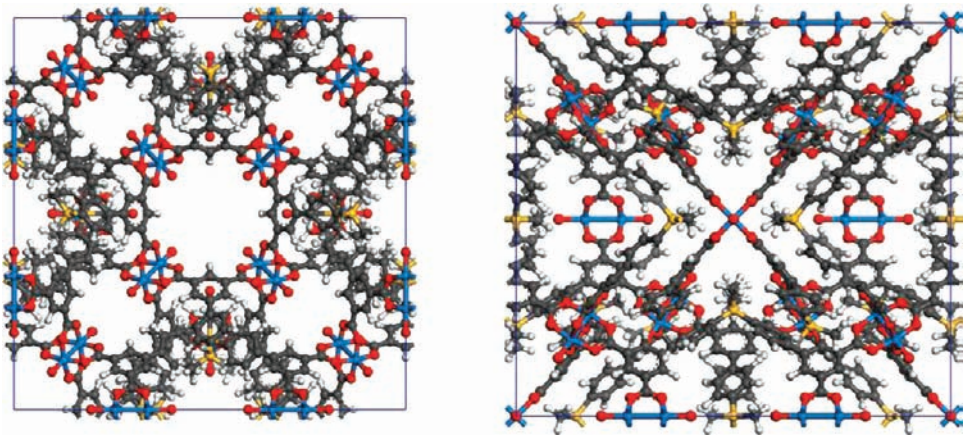

Figure 3. Unit cell with a view along the *c*-axis (left) and with a view along the *a*-axis (right); gray: carbon, white: hydrogen, red: oxygen, blue: copper, and yellow: silicon.

(apart from a zero shift of approximately 0.1° 2θ). Therefore, it can be confidently assumed that the structural model is correct. The remaining differences can probably be attributed to (i) the moderate crystallinity of the samples in conjunction with the limited resolution of the experimental XRD as the measurements were carried out on a usual laboratory X-ray diffractometer only; (ii) the fact that the solvent was not accounted for in the structural model.[34] After the solvent exchange activation procedure (48 h methanol and 48 h dichloromethane) a notable loss of long-range order of at least some structural parts of the framework can be observed. This is often the case, in particular for structures in which parts of the solvent molecules were coordinated to the metal center before. However, the XRD pattern of the solvent-exchanged form shows that the general structural features are preserved.

Structural Description. The structure of UHM-6 is a 2-fold interpenetrated structure. The two frameworks are related to each other by a translation of ($^1/_2$, $^1/_2$, $^1/_2$) (see Figure 2 and 3). Similar to the mdip linker in PCN-12,[16] the sbbip linker assumes two different conformations in the structure of UHM-6: In the first conformer, which has C_s symmetry, the four carboxylate groups lie within one plane. In the second conformer, the pairs of carboxylate groups attached to one phenyl ring face each other, resulting in a C_2 symmetry (Figure 4). Within a single framework, the cuboctahedral arrangement of Cu_2 paddle wheels is a prominent feature, which can be used as a starting point to understand the connectivity: One cuboctahedron is connected to the neighboring cuboctahedra by linkers assuming the C_s conformation along the *a*- and *b*-axis, whereas linker molecules with C_2 symmetry connect the cuboctahedra along the *c*-axis.

In comparison to PCN-12, the framework topology of UHM-6 is somewhat less complex. PCN-12 contains two nonequivalent types of cuboctahedral cages, whereas all cuboctahedra are equivalent by symmetry in UHM-6. The fact that different structures are formed by very similar linker molecules can be explained with the conformational properties of the linkers: A UHM-6-type structure cannot be realized with the shorter linker of PCN-12, because a conformation with both phenyl rings lying in one plane is sterically unfavorable. Moreover, the fact that PCN-12 possesses a noninterpenetrated structure, whereas UHM-6 exhibits interpenetration, is clearly related to the different dimensions of the linker molecules: The longer linker molecules of UHM-6 lead to the formation of large voids within one framework, which can readily accommodate a second framework.

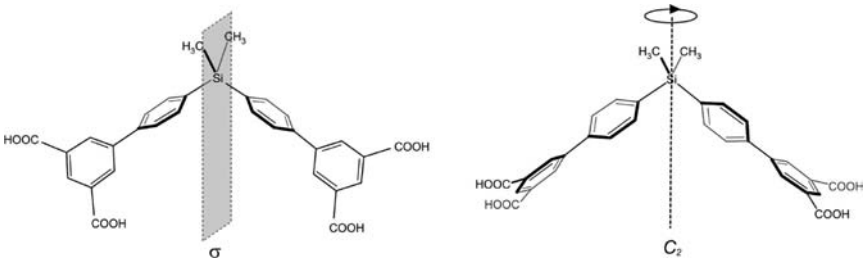

Figure 4. Two different conformations of the linker in the structure of UHM-6. In the first conformer, the four carboxylate groups lie within one plane (left, C_s symmetry) and in the second conformer, the pairs of carboxylate groups attached to one phenyl ring face each other (right, C_2 symmetry).

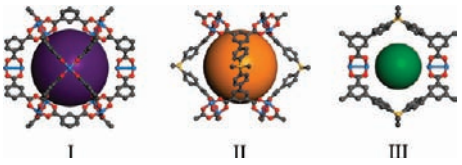

Figure 5. Three different pore types of UHM-6; gray: carbon, red: oxygen, blue: copper, and yellow: silicon.

In analogy to PMOF-3,[33] there are three different pore types in UHM-6, which are visualized in Figure 5. The first pore type, which is centered around the origin, corresponds to the cuboctahedral arrangement of Cu_2 paddle wheels mentioned previously, with the copper centers pointing into the pore. The pore diameter amounts to approximately 13 Å. The second pore type, which lies at the cell edges parallel to the *c*-axis, is surrounded by eight paddle wheels and four linker molecules having C_2 symmetry. It has dimensions of approximately 10 × 19 Å. Within each of the two frameworks, pores of type I lie at the corners of a cuboid, and are connected by pores of type II along the *c*-axis. Moreover, there is a third pore type, which is bordered by two paddle wheels that are connected by four linkers with C_s symmetry. These irregularly shaped pores are located at the *a*- and *b*-edges of the unit cell. It is noteworthy that the pore types I and II show a remarkable similarity to the two most prominent pore types observed in the structure of PCN-12/PCN-12-Si that were discussed in detail in previous work.[16,17]

The pore connectivity of UHM-6 can best be assessed from a visualization of the geometric surface area. The accessible surface area was calculated with Accelrys Materials Studio package 4.4, assuming a probe molecule radius of 1.84 Å, a value that corresponds to the kinetic radius of nitrogen.[25] Converted into macroscopic quantities, the surface area amounts to 1181 m^2/g, a value that is in very good agreement with the BET surface area determined experimentally. The accessible surface area is shown in Figure 2. Pores of type I and II belonging to the same framework are connected via the square faces of the cuboctahedra that lie perpendicular to the *c*-axis, leading to the formation of straight channels running along the [001] direction. Moreover, pore types I and II belonging to different frameworks are connected via the other four square faces of the cuboctahedra, forming channels running along the [110] direction. In total, the interconnected pore types I and II of both frameworks form a single three-dimensional network of straight channels. From a representation of the structure, for example, the one given in Figure 2 or 6, it could be expected that a second, independent system of straight channels running along the *c*-axis is formed by pore type III. However, the analysis of the surface area reveals that these channels are too narrow to be accessible to adsorbed molecules. Therefore, the pore type III described above does not correspond to actual pores, but inaccessible voids in the structure.

Gas Sorption Studies. *N_2 and Ar Physisorption measurements.* To remove the solvent used during the synthesis UHM-6 was activated via solvent exchange. TG-DTA studies coupled with mass spectrometry (MS) were carried out with the *as synthesized* and the activated material to ensure that the activation is complete after the solvent exchange (see Supporting Information). The porosity of the activated form of UHM-6 is confirmed by nitrogen and argon physisorption measurements at 77 and 87 K, respectively (Figure 7). The analysis of the recorded type-I isotherms (typical for microporous materials) reveals a specific surface area of S_{BET} = 1164 $m^2\ g^{-1}$ for the nitrogen measurement (for comparison: PMOF-3,[33] BET surface area = 1840 $m^2\ g^{-1}$) and 1254 $m^2\ g^{-1}$ for the argon measurement. Both values are in very good agreement with the one expected from theoretical calculations (1181 $m^2\ g^{-1}$ for nitrogen physisorption and 1214 $m^2\ g^{-1}$ for argon physisorption). The broad hysteresis at higher relative pressures in both isotherms is probably caused by interparticular cavitation. The micropore volume was calculated at a relative pressure of 0.2 (d < 2 nm) and was found to be $V_{micropore}$ = 0.46 $cm^3\ g^{-1}$ (N_2) and $V_{micropore}$ = 0.50 $cm^3\ g^{-1}$ (Ar).

H_2, CH_4, and CO_2 Physisorption Measurements. For testing the gas storage capabilities of UHM-6, volumetric low pressure physisorption measurements with hydrogen at 77 , 87, and 97 K, methane at 293 K, and carbon dioxide at 273 and 298 K were performed. Up to a pressure of 1 bar at 77 K a hydrogen uptake of 1.8 wt % was observed, which is in good agreement with the simulation (Figure 8, left). The experimentally determined higher uptake at low pressure is probably due to the open metal sites that are not considered specifically during the simulation process. The value of 1.8 wt % is in the range of other MOFs with comparable surface areas, for example, IRMOF-13 or PCN-9(Co).[35−38] In comparison to PMOF-3 (2.1 wt %)[33] the hydrogen uptake is slightly lower. For calculating the isosteric heat of adsorption (q_{st}) hydrogen measurements at 77, 87, and 97 K were used. For low degrees of hydrogen loading (0.04 wt %) the isosteric heat of adsorption of UHM-6 is 8.0 kJ mol^{-1}, with higher coverage it decreases to 6.1 kJ mol^{-1} at 0.85 wt % (Figure 8, right). In comparison with other MOFs, whose q_{st} values lie in the range from 4 to 8 kJ mol^{-1}, this result is in the upper range, somewhat higher than that of MOF-5 (5.2 kJ mol^{-1})[39] or $Cu_3(btc)_2$ (6.6 kJ mol^{-1})[34] but, for example, comparable to that of MOF-74 (8.3 kJ mol^{-1})[34] and PMOF-3 (8.9 kJ mol^{-1}).[33] This result confirms the general observation that MOFs with unsaturated metal sites exhibit higher q_{st} values than MOFs without unsaturated metal sites. However, the fact

dx.doi.org/10.1021/ic201596x |*Inorg. Chem.* 2011, 50, 11055–11063

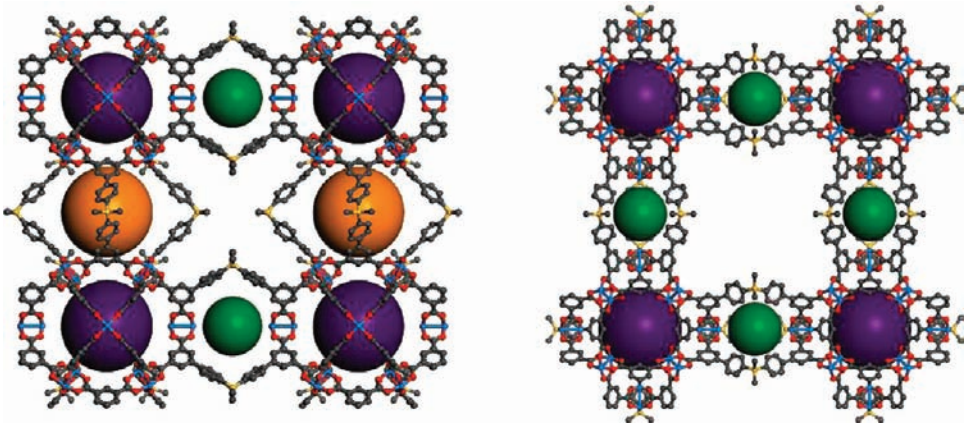

Figure 6. Combination of the three different pore types in UHM-6 within a single framework with a view along the *a*-axis (left) and with a view along the *c*-axis (right); gray: carbon, white: hydrogen, red: oxygen, blue: copper and yellow: silicon.

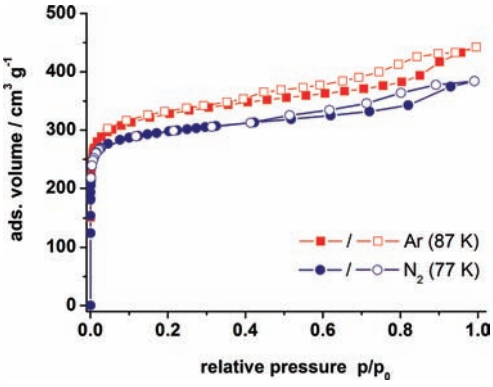

Figure 7. Nitrogen (77 K) and argon (87 K) physisorption isotherms of a UHM-6 sample after solvent exchange activation procedure (48 h methanol and 48 h dichloromethane). Filled symbols represent the adsorption and open symbols the desorption isotherms.

that the heat of adsorption of UHM-6 is nearly 1.5 times higher than that of $Cu_3(btc)_2$, even though both MOFs exhibit coordinatively unsaturated copper sites, indicates that further factors have to be taken into account which influence the heat of adsorption. In the case of UHM-6 the largest fraction of the accessible surface area is located around the channels running along the [001] and [110] direction (see Structural Description) which exhibit a relatively small diameter and could give rise to optimized vdW interactions. In addition, although speculative, the slightly higher polarizability of the silicon atoms in comparison to carbon atoms might contribute additionally to stronger dispersive interactions.

Methane and carbon dioxide physisorption measurements reveal that the activated form of UHM-6 exhibits a methane uptake of 0.8 mmol g^{-1} at 293 K and 1 bar and a carbon dioxide uptake of 3.3 mmol g^{-1} at 273 K (1 bar) and 2.1 mmol g^{-1} at 298 K (1 bar), respectively (see Figure 9). The uptake for CO_2 is considerably higher than for CH_4 (even if the slightly different temperatures are taken into account)[40] which is probably due to the higher quadrupole moment of carbon dioxide resulting in stronger interactions with the network. The value for the methane uptake at 1 bar and 293 K is comparable to the values published for $Cu_3(btc)_2$[41,42] but somewhat lower than the storage capacities of different mesoporous MILs.[43] The CO_2 uptake at 1 bar and 298 K is a bit smaller than in $Cu_3(btc)_2$.[40] In comparison with other low pressure CO_2 physisorption measurements UHM-6 exhibits similar behavior to the unmodified bio-MOF-1[44] but does not meet the best values published, that are in the range of 7−8 mmol g^{-1}.[42,45] Nonetheless, the CO_2 uptake (2.1 mmol g^{-1}) being almost three times higher than the CH_4 uptake (0.8 mmol g^{-1}) at room temperature provides potential for CO_2/CH_4 gas separation processes.

The isosteric heat of CO_2 adsorption dependence on the uptake is shown in Figure 10. The q_{st} values lie between 28 and 30 kJ mol^{-1} and are almost independent of the loading. These values are comparable to values of other MOFs with open copper sites, for instance $Cu_3(btc)_2$.[46]

Further studies concerning high pressure H_2, CO_2, and CH_4 physisorption measurements are currently underway.

GCMC Simulations. The adsorption isotherms obtained from the GCMC simulations are shown in Figure 8 and the Supporting Information. The calculated hydrogen adsorption isotherm at T = 77 K exhibits relatively good agreement with experimental data, although there is a pronounced tendency to underestimate the H_2 uptake by up to 0.3 wt %. This observation is most probably related to the presence of coordinatively unsaturated copper sites in UHM-6. As it has been discussed in detail in previous work,[26,47] simulations using standard force-field parameters are not able to capture the specific interaction of hydrogen with these sites. Therefore, the observed underestimation is not unexpected. The theoretical contribution of the metal sites in UHM-6 amounts to 0.6 wt %. However, a close inspection of the structure and the calculated surface area reveals that 50% of the copper sites point into regions of the structure that are not part of the accessible pore volume. Thus, the theoretical contribution is reduced to 0.3 wt %, which is in line with the observed deviation between simulation and experiment. The calculated isosteric heat of adsorption (see Supporting Information) in the limit of zero coverage amounts to 7.7 kJ mol^{-1}, and is thus slightly lower than the experimental value.

The calculated methane adsorption isotherm (Supporting Information) ranges slightly below the experimental isotherm. Again, these findings may be related to the interaction of CH_4 with the copper sites, which has been found to have a significant influence on the methane storage properties even at room temperature.[48] A similar effect could be expected for CO_2, since comparable simulations of CO_2 adsorption in $Cu_3(btc)_2$ exhibited a

dx.doi.org/10.1021/ic201596x |*Inorg. Chem.* 2011, 50, 11055–11063

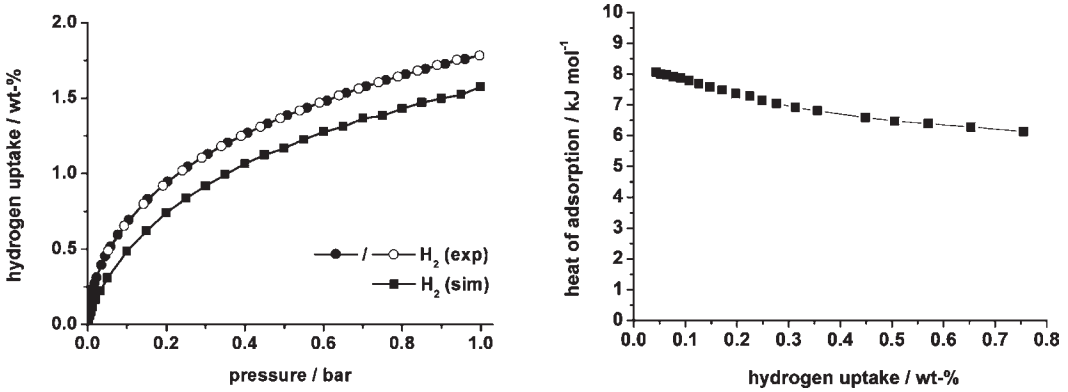

Figure 8. (left) Hydrogen physisorption isotherm (77 K) of a UHM-6 sample after solvent exchange activation procedure in comparison with the results of the GCMC simulation. Filled symbols: adsorption, open symbols: desorption isotherm. (right) Isosteric heat of hydrogen adsorption as a function of loading calculated from isotherms at 77, 87, and 97 K (the three isotherms are shown in the Supporting Information).

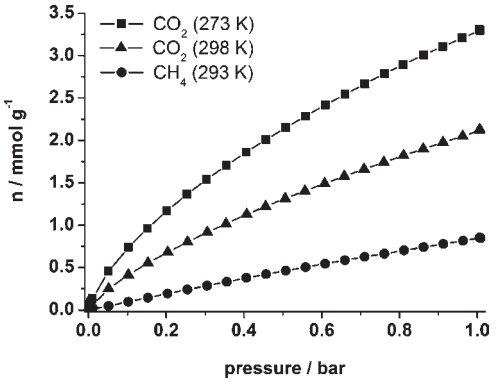

Figure 9. Methane (293 K) and carbon dioxide adsorption isotherms (298 and 273 K) of an activated UHM-6 sample.

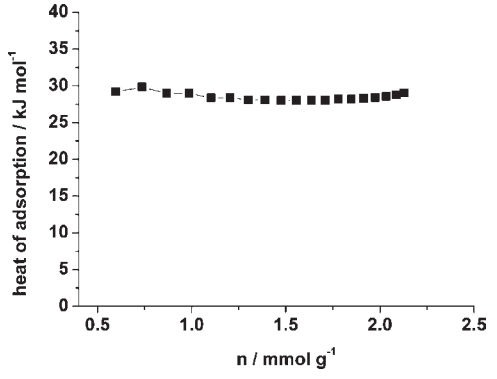

Figure 10. Isosteric heat of adsorption as a function of CO_2 uptake calculated from isotherms at 273 and 298 K.

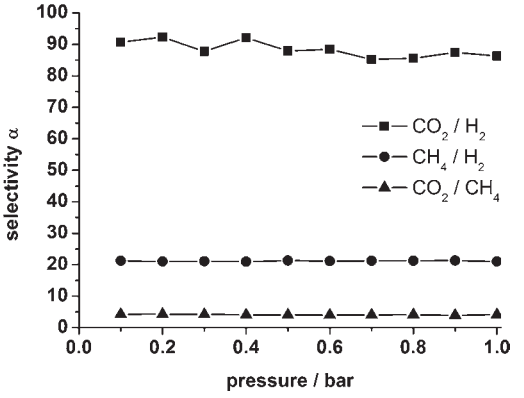

Figure 11. CH_4/H_2, CO_2/H_2, and CO_2/CH_4 selectivities calculated from binary mixture isotherms for T = 298 K, assuming an equimolar mixture composition.

significant underestimation of the carbon dioxide uptake when literature parameters were used.[49] Interestingly, this is not observed for UHM-6 (see Supporting Information). Conversely, the CO_2 uptake is slightly overestimated by the simulations at pressures above 0.8 bar. While the origin of these deviations cannot be elucidated in this context, they could be related to the approximations used in the representation of electrostatic interactions. Of the three species considered, electrostatic effects are most important for carbon dioxide, which is why inaccuracies of the electrostatic potential in the pores will mainly affect the CO_2 adsorption isotherm.

Finally, the CH_4/H_2, CO_2/H_2, and CO_2/CH_4 selectivities were calculated from binary mixture isotherms for T = 298 K, assuming an equimolar mixture composition (see Figure 11). The predicted CH_4/H_2 adsorption selectivity amounts to $\alpha \approx 21$. This value is slightly higher than the calculated CH_4/H_2 adsorption selectivity of $Cu_3(btc)_2$.[50] While lower selectivities have been obtained for different IRMOFs and ZIFs,[51] a higher selectivity of $\alpha \approx 150$ has been predicted for Zn(tbip).[52]

Concerning the separation of CO_2/H_2 mixtures, the selectivity of UHM-6 ($\alpha \approx 90$) is also moderate, ranging above typical IRMOFs,[50] but lying in the same range as the selectivity of $Cu_3(btc)_2$.[49] A much higher CO_2/H_2 selectivity (>1000) has been predicted for a MOF with an anionic framework and charge-balancing Na^+ cations.[53] Finally, the CO_2/CH_4 selectivity amounts to $\alpha \approx 4$. This selectivity is somewhat lower than the selectivity of $Cu_3(btc)_2$.[49] In total, the simulation results show that the incorporation of silicon atoms in the linker of UHM-6 has, at best, a moderate influence on the separation properties. Compared to MOFs like $Cu_3(btc)_2$, UHM-6 seems to have an enhanced affinity toward methane, which is reflected by an increased CH_4/H_2 selectivity and a reduced CO_2/CH_4 selectivity. Probably,

dx.doi.org/10.1021/ic201596x |Inorg. Chem. 2011, 50, 11055–11063

this behavior is caused by an increased dispersive interaction between the methane molecules, which have a relatively high polarizability, and the silicon atoms of the framework. A more detailed study of these interactions, however, would require ab initio methods.

CONCLUSIONS

In summary, a new MOF, called UHM-6, containing unsaturated copper sites and the nonlinear organosilicon linker sbbip was synthesized. The extension of the linker dmsdip, incorporated in the MOF PCN-12-Si (UHM-3), by two phenyl rings did not result in a framework having the same topology but larger voids; instead a 2-fold interpenetrated network is formed, which is isoreticular to PMOF-3. Physisorption measurements reveal that UHM-6 possesses a notably lower specific surface area than PMOF-3 (1200 vs 1840 $m^2 g^{-1}$). However, the hydrogen uptake of UHM-6 at 1 bar and 77 K is only slightly lower than for PMOF-3 (1.8 vs 2.1 wt %).The isosteric heat of adsorption values for these two MOFs exhibiting the same topology are similar, too. Conversely, this means that there are no indications that incorporation of linkers with atoms of higher polarizability than carbon (here silicon) are advantageous in terms of hydrogen storage capacities. However, it would be very interesting to compare UHM-3 or PCN-12 with a yet hypothetical UHM-6 having the same topology. The design and synthesis of new linkers exhibiting the same backbone but carrying additional side groups which might prevent the occurrence of interpenetration are currently planned.

Further physisorption experiments and supplemental GCMC simulations indicate that UHM-6 bear potential for usage in gas separation processes, in particular for CO_2/H_2 separation.

ASSOCIATED CONTENT

Supporting Information. (1) Synthesis scheme of the linker, (2) Thermal Analysis of UHM-6 (3), Physisorption isotherms, (4) GCMC simulations: Models of fluid molecules, (5) GCMC simulation: Framework atoms of UHM-6, (6) Calculation of ESP charges, (7) Binary mixture isotherms for $T = 298$ K. This material is available free of charge via the Internet at http://pubs.acs.org.

AUTHOR INFORMATION

Corresponding Author

*E-mail: michael.froeba@chemie.uni-hamburg.de. Phone: +49-40-42838-3103. Fax: +49-40-42838-6348.

ACKNOWLEDGMENT

D.F. thanks the Graduate School for Resource and Energy Management "C1-REM" (Excellence Initiative of the Federal State Hamburg) and M.F. the DFG Interdisciplinary Graduate School 611 "Design and Characterization of Functional Materials" for financial support.

REFERENCES

(1) Yang, J.; Sudik, A.; Wolverton, C.; Siegel, D. J. *Chem. Soc. Rev.* **2010**, *39*, 656–675.

(2) EERE: Hydrogen, Fuel Cells, & Infrastructure Technologies Program. Homepage, http://www.eere.energy.gov/hydrogenandfuelcells/ (accessed 2011).

(3) Long, J. R.; Yaghi, O. M. *Chem. Soc. Rev.* **2009**, *38*, 1213–1214.

(4) Kitagawa, S.; Kitaura, R.; Noro, S. *Angew. Chem., Int. Ed.* **2004**, *43*, 2334–2375.

(5) Ferey, G. *Chem. Soc. Rev.* **2008**, *37*, 191–214.

(6) Davis, M. E. *Nature* **2002**, *417*, 813–821.

(7) Lee, J. Y.; Farha, O. K.; Roberts, J.; Scheidt, K. A.; Nguyen, S. T.; Hupp, J. T. *Chem. Soc. Rev.* **2009**, *38*, 1450–1459.

(8) Li, J. R.; Kuppler, R. J.; Zhou, H.-C. *Chem. Soc. Rev.* **2009**, *38*, 1477–1504.

(9) Morris, R. E.; Wheatley, P. S. *Angew. Chem., Int Ed.* **2008**, *47*, 4966–4981.

(10) Ma, S.; Zhou, H.-C. *Chem. Commun.* **2010**, *46*, 44–53.

(11) http://www1.eere.energy.gov/hydrogenandfuelcells/storage/pdfs/targets_onboard_hydro_storage.pdf (accessed 2011).

(12) Frost, H.; Düren, T.; Snurr, R. Q. *J. Phys. Chem. B* **2006**, *110*, 9565–9570.

(13) Dinca, M.; Long, J. R. *Angew. Chem., Int. Ed.* **2008**, *36*, 6766–6779.

(14) Dinca, M.; Long, J. R. *J. Am. Chem. Soc.* **2005**, *127*, 9376–9377.

(15) Dinca, M.; Dailly, A.; Liu, Y.; Brown, C. M.; Neumann, D. A.; Long, J. R. *J. Am. Chem. Soc.* **2006**, *128*, 16876–16883.

(16) Wang, X.-S.; Ma, S.; Forster, P. M.; Yuan, D.; Eckert, J.; L opez, J. J.; Murphy, B. J.; Parise, J. B.; Zhou, H.-C. *Angew. Chem., Int. Ed.* **2008**, *47*, 7263–7266.

(17) Wenzel, S. E.; Fischer, M.; Hoffmann, F.; Fröba, M. *Inorg. Chem* . **2009**, *48*, 6559–6565.

(18) Wenzel, S. E.; Hoffmann, F.; Fröba, M. *Inorg. Chem.*, submitted for publication.

(19) Ma, S.; Sun, D.; Ambrogio, M.; Fillinger, J. A.; Parkin, S.; Zhou, H.-C. *J. Am. Chem. Soc.* **2007**, *129*, 1858–1859.

(20) Pan, L.; Olson, D. H.; Ciemnolonski, L. R.; Heddy, R.; Li, J. *Angew. Chem., Int. Ed.* **2006**, *45*, 616–619.

(21) Pan, L.; Sander, M. B.; Huang, X.; Li, J.; Smith, M.; Bittner, E.; Bockrath, B.; Johnson, J. K. *J. Am. Chem. Soc.* **2004**, *126*, 1308–1309.

(22) Kwak, G.; Masuda, T. *Macromolecules* **2002**, *35*, 4138–4142.

(23) Ghatge, N. D.; Jadhav, J. Y. *Synth. React. Inorg. Met.-Org. Chem.* **1984**, *14*, 83–96.

(24) Düren, T.; Bae, Y.-S.; Snurr, R. Q. *Chem. Soc. Rev.* **2009**, *38*, 1237–1247.

(25) *Materials Studio*, v4.4; Accelrys Inc.: San Diego, CA, 2008.

(26) Fischer, M.; Hoffmann, F.; Fröba, M. *ChemPhysChem.* **2009**, *10*, 2647–2657.

(27) Rappe, A. K.; Casewit, C. J.; Colwell, K. S.; Goddard, W. A.; Skiff, W. M. *J. Am. Chem. Soc.* **1992**, *114*, 10024–10035.

(28) Singh, U. C.; Kollman, P. A. *J. Comput. Chem.* **1984**, *5*, 129–145.

(29) Buch, V. *J. Chem. Phys.* **1994**, *100*, 7610–7629.

(30) Martin, M. G.; Siepmann, J. I. *J. Phys. Chem. B* **1998**, *102*, 2569–2577.

(31) García-Sánchez, A.; Ania, C. O.; Parra, J. B.; Dubbeldam, D.; Vlugt, T. J. H.; Krishna, R.; Calero, S. *J. Phys. Chem. C* **2009**, *113*, 8814–8820.

(32) Loiseau, T.; Mellot Draznieks, C.; Muguerra, H.; Ferey, G.; Haouas, M.; Taulelle, F. *C. R. Chim.* **2005**, *8*, 765–772.

(33) Liu, X.; Park, M.; Hong, S.; Oh, M.; Yoon, J. W.; Chang, J.-S.; Lah, M. S. *Inorg. Chem.* **2009**, *48*, 11507–11509.

(34) Although according to our experience the influence of the solvent on the reflection intensities is usually not very significant, we must note that the solvent might play a non-negligible role in the present case. As the solvent is typically completely disordered there is no simple way to include it into the structural model. (An attempt to carry out a Rietveld refinement did not result in an improved, more plausible structural model.)

(35) Rowsell, J. L. C.; Yaghi, O. M. *J. Am. Chem. Soc.* **2006**, *128*, 1304–1315.

(36) Rowsell, J. L. C.; Millward, A. R.; Park, K. S.; Yaghi, O. M. *J. Am. Chem. Soc.* **2004**, *126*, 5666–5667.

(37) Ma, S.; Zhou, H.-C. *J. Am. Chem. Soc.* **2006**, *128*, 11734–11735.

(38) Chun, H.; Dybtsev, D. N.; Kim, H.; Kim, K. *Chem.—Eur. J.* **2005**, *11*, 3521–3529.

(39) Kaye, S. S.; Long, J. R. *J. Am. Chem. Soc.* **2005**, *127*, 6506–6507.
(40) Because of technical reasons, it was not possible to perform the measurements for CO_2 and CH_4 at exactly the same temperature.
(41) Wang, Q. M.; Shen, D.; Bülow, M.; Lau, M. L.; Deng, S.; Fitch, F. R.; Lemcoff, N. O.; Semanscin, J. *Microporous Mesoporous Mater.* **2002**, *55*, 217–230.
(42) Wu, H.; Simmons, J. M.; Liu, Y.; Brown, C. M.; Wang, X.-S.; Ma, S.; Peterson, V. K.; Southon, P. D.; Kepert, C. J.; Zhou, H.-C.; Yildirim, T.; Zhou, W. *Chem.—Eur. J.* **2010**, *16*, 5205–5214.
(43) Llewellyn, P. L.; Bourrelly, S.; Serre, C.; Vimont, A.; Daturi, M.; Hamon, L.; De Weireld, G.; Chang, J.-S.; Hong, D.-Y.; Hwang, Y. K.; Hwa Jhung, S.; Férey, G. *Langmuir* **2008**, *24*, 7245–7250.
(44) An, J.; Rosi, N. L. *J. Am. Chem. Soc.* **2010**, *132*, 5578–5579.
(45) Caskey, S. R.; Wong-Foy, A. G.; Matzger, A. J. *J. Am. Chem. Soc.* **2008**, *130*, 10870–10871.
(46) Moellmer, J.; Moeller, A.; Dreisbach, F.; Glaeser, R.; Staudt, R. *Microporous Mesoporous Mater.* **2011**, *138*, 140–148.
(47) Fischer, M.; Kuchta, B.; Firlej, L.; Hoffmann, F.; Fröba, M. *J. Phys. Chem. C* **2010**, *114*, 19116–19126.
(48) Getzschmann, J.; Senkovska, I.; Wallacher, D.; Tovar, M.; Fairen-Jimenez, D.; Düren, T.; van Baten, J. M.; Krishna, R.; Kaskel, S. *Microporous Mesoporous Mater.* **2010**, *136*, 50–58.
(49) Fischer, M.; Hoffmann, F.; Fröba, M. *ChemPhysChem.* **2010**, *11*, 2220–2229.
(50) Yang, Q.; Zhong, C. *J. Phys. Chem. B* **2006**, *110*, 17776–17783.
(51) Keskin, S. *J. Phys. Chem. C* **2011**, *115*, 800–807.
(52) Liu, J.; Johnson, J. K. *J. Low Temp. Phys.* **2009**, *157*, 268–276.
(53) Babarao, R.; Jiang, J. *J. Am. Chem. Soc.* **2009**, *131*, 11417–11425.